Low Density Lipoprotein Receptor-Related Protein 1 (LRP1) is a host factor for RNA viruses including SARS-CoV-2

Stephanie Devignot[1], Tim Wai Sha[1], Thomas Burkard[2], Patrick Schmerer[1], Astrid Hagelkruys[2], Ali Mirazimi[3,4], Ulrich Elling[2], Josef M. Penninger[2,5*], Friedemann Weber[1,6*]

[1] Institute for Virology, FB10-Veterinary Medicine, Justus-Liebig University, Giessen, Germany

[2] Institute of Molecular Biotechnology of the Austrian Academy of Sciences (IMBA), Vienna, Austria

[3] Public Health Agency of Sweden, Solna, Sweden

[4] Department of Laboratory Medicine, Karolinska Institutet, Sweden

[5] Department of Medical Genetics, Life Sciences Institute, University of British Columbia, Vancouver, Canada

[6] German Centre for Infection Research (DZIF), partner site Giessen, Germany

*corresponding authors: josef.penninger@ubc.ca; friedemann.weber@vetmed.uni-giessen.de

Running title: LRP1 supports the replication cycle of a broad spectrum of RNA viruses

Key words: LRP1, CD91, host cell factor, RNA virus, Rift Valley fever virus, bunyavirus, SARS-CoV-2

Abstract

Viruses with an RNA genome are the main causes of zoonotic infections. In order to identify novel pro-viral host cell factors, we screened a haploid insertion-mutagenized mouse embryonic cell library for clones that rendered them resistant to the zoonotic Rift Valley fever virus (RVFV; family *Phleboviridae*, order *Bunyavirales*). This screen returned the Low Density Lipoprotein Receptor-Related protein 1 (LRP1, or CD91) as top hit, a 600 kDa plasma membrane protein known to be involved in a wide variety of cell activities. Inactivation of LRP1 expression in human cells reduced RVFV infection at the early stages of infection, including the particle attachment to the cell. In the highly LRP1-positive human HuH-7 cell line, LRP1 was required for the early infection stages also of Sandfly fever Sicilian virus (SFSV; family *Phleboviridae*, order *Bunyavirales*), vesicular stomatitis (VSV; family *Rhabdoviridae*, order *Mononegavirales*), Encephalomyocarditis virus (EMCV, family *Picornaviridae*), and the coronaviruses MERS-CoV, SARS-CoV-1, and SARS-CoV-2. While for RVFV, EMCV, and MERS-CoV the replication cycle could eventually catch up, LRP1 requirement for the late infection stage in HuH-7 cells was observed for SFSV, La Crosse virus (LACV; family *Peribunyaviridae*, order *Bunyavirales*), VSV, SARS-CoV-1, and SARS-CoV-2. For SARS-CoV-2, the absence of LRP1 stably reduced viral RNA levels in human lung Calu-3 cells, and both RNA levels and particle production in the hepatic HuH-7 cells. Thus, we identified LRP1 as a host factor that supports various infection cycle stages of a broad spectrum of RNA viruses.

Introduction

Most pandemics, epidemics, and zoonotic spillover infections are caused by enveloped RNA viruses (1-3). These pathogens contain an RNA genome of positive-sense or negative-sense polarity that is encapsidated by a viral nucleoprotein and surrounded by a lipid bilayer containing transmembrane glycoproteins. Although RNA viruses are phylogenetically very diverse, it is conceivable that all are depending on common basic factors of the cell.

Rift Valley fever virus (RVFV; family *Phleboviridae*, order *Bunyavirales*) is an emerging zoonotic negative-strand RNA virus (4) that is listed by the WHO among the pathogens posing the greatest public health risk (2). Using RVFV as a model, we aimed to identify host cell factors supporting the replication cycle of RNA viruses. An insertion-mutagenized haploid cell library was screened for clones with resistance to the highly cytopathogenic RVFV as an indication that the deleted gene is essential for viral replication. As top ranking hit emerged the Low Density Lipoprotein Receptor-Related protein 1 (LRP1), a large plasma membrane receptor that can bind and internalize more than 40 different ligands. Indeed, a lack of LRP-1 reduced the ability of RVFV to attach to the cell surface and enter the cytoplasm, whereas RNA levels seemed not to be affected. Subsequent experiments using human HuH-7 knockout cells revealed that LRP1 is also a host cell factor for other, RVFV-related and –unrelated RNA viruses, most prominently human pathogenic coronaviruses SARS-CoV-1 and SARS-CoV-2. Depending on the particular virus, however, LRP1 was important for different infection steps ranging from particle attachment to late-stage viral RNA synthesis. Our study may thus establish LRP-1 as a broad-band host factor for many RNA viruses that acts not exclusively on attachment but in some cases at later stages of the replication cycle. Moreover, we show that SARS-coronaviruses are among the most LRP1-dependent viruses.

Results

Forward genetic screen for genes supporting RVFV infection

As RVFV is highly cytolytic, we devised a forward genetic screen that is based on the positive selection of cells deficient in pro-viral genes. A genome-wide library of knockout haploid mouse embryonic stem cells (mESCs), derived from parthenogenetic mouse embryos, was generated by mutagenizing with a retroviral genetrap (Fig. 1A) that disrupts genes in a revertible manner (5). Altogether 5*10E8 cells were mutagenized by transduction with a genetrap retrovirus at an MOI of 0.02 resulting in approximately 10E7 independent mutations, selected by neomycin and expanded. Infection of the parental, non-mutagenized haploid mESCs with the attenuated RVFV strain MP-12 was productive (Fig. S1A) and caused cytopathic effect (CPE) (Fig. S1B). Also after infection of the ~75 million genetrap library cells (7.5 cells/mutation) most of the mutagenized mESCs underwent CPE, but surviving and proliferating cell clones became enriched over 17 days under infection pressure. After repeated cycles of infection and selection (Figs. 1B and S2), all the surviving cell clones were collected, and the mutagenized genes then identified by an inverted PCR / restriction digest assay on genomic cell DNA, followed by Next Generation Sequencing (Fig. S3A and B, table S1). The top-ranking gene, found to be genetrap-inserted many times independently (Fig. S4), was Low Density Lipoprotein Receptor-Related protein 1 (LRP1). LRP1 is an approximately 600 kDa plasma membrane protein with a 515 kDa extracellular part (6-10). For validation, we employed our genome-wide Haplobank library of more than 100,000 haploid mESC clones that contain a revertible genetrap with individual barcodes (Fig. 2A) (5). We took a number of independent Haplobank clones that carried a genetrap insertion in an intron of LRP1 (table 1). Moreover, Cre-Lox inversion of the genetrap was performed, so each clone exists in a wt and a knockout version (sister clones) (Fig. 2B). The mutant or wt mESC clones from the Haplobank and their respective reverted sister clones, each labelled either with GFP or mCherry, respectively (see table 1), were then mixed at a 3:7 ratio and subjected to a growth competition assay under RVFV MP-12 infection. Figure 2C shows how LRP1-mutated cell clones exhibit a growth advantage if kept under RVFV MP-12 infection. As controls, we employed Haplobank cell clones mutated in previously identified pro-viral host factors of RVFV, namely prenyltransferase alpha subunit repeat containing 1 (PTAR1; Fig. 2D) (11), and the E3 ubiquitin ligase FBXW11 (Fig. 2E) (12, 13). Interestingly, in our mESC system the inactivation of these published control genes presented a much weaker survival benefit under selection pressure by RVFV than the deletion of LRP1.

LRP1 impacts intracellular RNA levels of RVFV, but neither protein synthesis nor particle production

To follow up our findings from the mouse ESCs, we performed siRNA knockdown of LRP1 in human A549 cells and tested its effect on RVFV MP-12 replication using RT-qPCR. siRNA-mediated downmodulation of LRP1 mRNA (Fig. S5A) resulted in an up to 50% reduction of RVFV gene

expression at 5 h and 24 h p.i. (Fig. 3A). Immunoblot analysis however revealed that A549 cells express comparatively little LRP1, whereas in human HuH-7 cells both the 515 kDa alpha chain as well as the 85 kDa beta chain gave strong signals (Fig. S5B). Thus, we robustly downregulated LRP1 levels in the HuH-7 cells by introducing a CRISPR/Cas9 knockout (table S2 and Fig. S5B), and studied its phenotype with regard to RVFV replication. Also in the HuH-7 LRP1 knockout cells RT-qPCR analysis showed a suppression of viral gene expression by more than 50% already at 5 p.i. (Fig. 3B). However, immunoblotting revealed that levels of viral nucleocapsid (N) protein were unchanged between wt and LRP1 knockout cells (Fig. 3C). Moreover, when supernatants from the cells infected with MOI 0.01 were titrated, we did not observe any differences in virus yields. From these data we concluded that LRP1 is important for maintaining intracellular RNA levels of RVFV in human cells, but that its absence has no consequences for the production of progeny virus particles.

LRP1 acts early in the viral infection cycle

The results obtained so far may indicate that LRP1 is already important at 5 h p.i.. For RVFV, the replication cycle is initiated by attachment of particles to the cell, followed by their endosomal internalisation, fusion of viral and endosomal membranes, and entry of the nucleocapsids into the cytoplasm (4). In order to identify the earliest virus replication step that involves LRP1, we infected HuH-7 wt and LRP1 knockout cells in a synchronized manner, and took cell-associated RNA samples at 0 h (attachment), 2 h (internalisation), 5 h (gene expression after entry into the cytoplasm) and 24 h (late phase of replication). For these analyses we engaged the wt RVFV strain ZH548 which unlike MP-12 is virulent for humans and animals. As shown in figure 4, LRP1 is required already for the attachment of RVFV particles to the cells, and viral RNA levels in the mutant cells lag behind in the subsequent infection stages up to the 5 h p.i. time point. At the 24 h time point, however ZH548 RNA synthesis has recovered in the LRP1 knockout cells, different from what was observed to the attenuated mutant strain MP-12 (see Fig. 3A and B). Thus, is LRP1 is robustly supporting the immediate-early steps of RVFV infection.

LRP1 has a broad relevance for RNA viruses

The results from the knockout and time course experiments indicate a role of LRP1 as co-factor rather than as a main receptor of RVFV infection. We tested its importance for other RNA viruses, namely the closely related Sandfly fever Sicilian virus (SFSV; family *Phleboviridae*, order *Bunyavirales*), the more remotely related La Crosse bunyavirus (LACV; family *Peribunyaviridae*, order *Bunyavirales*), and the non-related vesicular stomatitis (VSV; family *Rhabdoviridae*, order *Mononegavirales*). Moreover, as these all are negative-strand RNA viruses, we additionally included the non-enveloped, positive-stranded Encephalomyocarditis virus (EMCV, family *Picornaviridae)*, and the three human pathogenic members of the positive-strand RNA virus family *Coronaviridae*, namely MERS-CoV, SARS-CoV-1, and SARS-CoV-2. As shown in figure 5A, for SFSV LRP1 is involved already in particle attachment,

as for RVFV. By contrast, for the more remotely related LACV the lack of LRP1 has only a significant impact at 24 h p.i. (Fig. 5B). The Rhabdovirus VSV, is also affected at 24 h p.i., but additionally at the attachment step (Fig. 5C). For the picornavirus EMCV, an LRP1-dependency was only apparent at the attachment step of the infection cycle, whereas already at 2 h pi LRP1 was not required any more (Fig. 5D). For MERS-CoV, the LRP1 knockout impacted particle attachment and the following early steps, but was compensated at 24 h p.i. (Fig. 5E). The most striking phenotype was however exhibited by the two SARS-coronaviruses, namely SARS-CoV-1 which caused a pandemic in 2002/2003, and the recently emerged SARS-CoV-2. Here, all steps from particle attachment up until the late-stage virus RNA levels at 24 h p.i. were impacted by the lack of LRP1 (Figs. 5F and G). In fact, while for all other tested viruses the typical reduction in viral RNA was around 50% and remained mostly stable or even caught up during the infection cycle, for both SARS-coronaviruses the RNA levels remained low over time, resulting in a 50 to over 95% reduction relative to the LRP1-expressing wt cells at 24 h p.i..

Our comparative time course experiments in HuH-7 cells thus demonstrate that LRP1-dependency is a common trait among RNA viruses. In most cases LPR1 is facilitating virus attachment, and its absence has a rather transient effect on virus infection. For some viruses, however, also the late stage RNA synthesis depends partially or – as is the case for the two SARS-coronaviruses – substantially on the presence of an intact LRP1.

SARS-CoV-2 progeny particle production in cells lacking LRP1

For SARS-CoV-2, the causative agent of COVID-19, we further characterized the impact of LRP1 deficiency. To this aim, we employed siRNA knockdown in Calu-3 (Fig. S6A), a prototypical human lung epithelial cell line used in SARS-CoV-2 research. In these cells, LRP1 was found to be supporting RNA synthesis at 5 h p.i and 24 h p.i, but not at the earlier stages of the replication cycle (Fig. 6A). Moreover, an – albeit transient – impact on viral N protein synthesis could be observed (Fig. 6B). Despite these clear effects on late stages of SARS-CoV-2 infection, however, virus yields were comparable between wt and LRP1-deficient Calu-3 cells at all time points measured (Fig. 6C).

As observed previously for the human alveolar basal epithelial cell line A549 (see Fig. S5), Calu-3 cells express very little LRP-1 (Fig. S6B). For further investigations, we therefore returned to the HuH-7 cells, which had exhibited both higher LRP1 levels and a more profound impact of LRP1 deficiency on the SARS-CoV-2 replication cycle (see Fig. 5G). Strikingly, analyses of an infection time course demonstrated that in this system an LRP1 deficiency robustly impacted expression of the viral nucleocapsid protein (N) (Fig. 7A) as well as virus yields in the supernatants (Fig. 7B), and the effects were observed throughout the entire replication cycle. In fact, virus yields did not even recover towards the end of the infection cycle, indicating a strong dependency on LRP1. Of note, a markedly reduced SARS-CoV-2 replication was also observed for two other HuH-7 LRP1 knockout cell clones, excluding clonal effects (Fig. 7C).

Thus, taken together, our forward genetic screen in haploid mESCs enabled us to identify the cellular

protein LRP1 as a host factor for RVFV and a series of other RNA viruses, most prominently SARS-CoV-2. Although the strength of the pro-viral effect of LRP1 was cell type-dependent, for most viruses already the attachment phase of the replication cycle was involved. Interestingly, in some cases (e.g. SARS-CoV-2) LRP1 had an impact on the late phase of infection, indicating a role as an auxiliary factor also in RNA synthesis.

Discussion

LRP1 (or CD91) is a scavenger-type receptor involved in a wide variety of cell activities like migration, proliferation, differentiation, but also regulation of cholesterol homeostasis, inflammation, or clearance of plasma proteins from the blood stream (6-10). It is important for the integrity of blood-brain barrier and can bind and internalize more than 40 different ligands (including apoptotic bodies or the Alzheimer disease-associated tau protein). Moreover, LRP1 modulates signalling pathways like e.g. those by JAK/STAT, ERK1/2 or TGF-ß (10, 14). Our findings indicate that many viruses are aided by LRP1 at their attachment and entry step, as might be expected from a membrane protein involved in constitutive endocytosis. In agreement with these findings, a recent study (published while our manuscript was in preparation) showed that LRP1 acts as a receptor of RVFV by binding to the viral envelope protein and mediating its entry into the cytoplasm (15).

Interestingly however, some viruses – including SARS-CoV-2 - also require LRP1 for the later stages of infection. Like all positive-stranded RNA viruses, coronaviruses are known to intensively reorganize internal cell membranes in order to generate compartments that can serve as a safe space for transcription and replication of the genome RNA, and to assemble progeny particles (16-18). As LPR1 is mostly cycling between the plasma membrane and the endosomes, it may transport factors critical for the RNA replication of SARS-coronaviruses, e.g. lipids required for the formation of virally-induced intracellular membrane compartments. Curiously, in HuH-7 cells the late-stage requirement for LRP1 was only present for SARS-CoV-1 and SARS-CoV-2 (subgenus *Sarbecovirus*, genus *Betacoronavirus*), but not for the related MERS-CoV (subgenus *Merbecovirus*, genus *Betacoronavirus*) (19), while the early-stage requirement for LRP1 was observed for both these betacoronavirus subgenera. It is hence possible that the SARS-coronaviruses engage LRP1 for two different viral activities, attachment and late-stage replication, whereas for MERS-CoV it may be only attachment or, alternatively, the requirement for the later infections stages is not as strict as for the SARS-coronaviruses.

SARS-CoV-2 exhibited the most profound LRP1-dependency in the hepatic HuH-7 cells, impacting both the early attachment step and the subsequent RNA synthesis. HuH-7 cells are of hepatic origin (20), and SARS-CoV-2 is capable of infecting and damaging organs including the liver (21-23). Besides the liver, LRP1 is also detectable in tissues like brain, respiratory system, kidney, sexual organs and connective and soft tissues (24). Cell types with highest LRP1 levels are hepatocytes, Leydig cells, brain cells like microglia and astrocytes, syncytiotrophoblasts, skeletal myocytes, fibroblasts, peritubular cells, and monocytes/macrophages (25). Future studies may reveal whether in these and other cell types LRP1 is contributing to the cell tropism of SARS-CoV-2.

In Calu-3 cells, LRP1 was neither required early in infection nor for virus yields, but exclusively for late-stage RNA synthesis. Like Calu-3, alveolar cells and other epithelial cells express much lower levels of LRP1 as hepatocytes, indicating that factors other than LRP1 are mainly supporting SARS-CoV-2 attachment and entry. Thus, apparently, early-stage LRP1 usage by SARS-CoV-2 is cell type-dependent, whereas the late-stage requirement for RNA synthesis is general.

Taken together, we have identified LRP1 as a broadly active pro-viral factor that enables entry of RNA viruses. In some cases, most prominently SARS-CoV-1 and SARS-CoV-2, LRP1 is also facilitating the late stage of infection. It will be interesting to find out how SARS-coronaviruses are engaging LRP1 for their intracellular replication, and by which alternative mechanism MERS-CoV is circumventing LRP1 at the late stage of infection.

Materials and Methods

Cells and viruses

A549, BHK, HuH-7, Vero E6, Vero B4, as well as Calu-3 (kindly provided by Marcel Müller, Berlin, Germany) and LRP-1 knockout HuH-7 cells were grown in Dulbecco's modified Eagle's medium (DMEM) containing 10% foetal calf serum (FCS), 2 mM glutamine, 100 U/ml penicillin, and 100 µg/ml streptomycin. Medium and supplements were purchased from Thermo Fisher Scientific. The mouse haploid embryonic stem cells AN3-12 were derived and sorted for their haploidy as described (26, 27). The AN3-12 cells, the AN3-12 genetrap-mutated library, and the derived genetrap-mutated specific cell lines from the Haplobank (5) were grown in embryonic stem cell medium (ESCM) containing FCS and mouse Leukemia Inhibitory Factor (LIF) (5). All AN3-12 cells were cultured in 10 cm cell culture dishes, passaged every second day by trypsinizing and re-seeding at 1:10, and the medium changed every other day.

Rift Valley fever virus (RVFV) strain MP-12, LaCrosse virus (LACV), Encephalomyocarditis virus strain FA (EMCV), and Vesicular Stomatitis Virus (VSV) were propagated in BHK cells. Recombinant RVFV (strain ZH548), Severe Acute Respiratory Syndrome Coronavirus 1 (SARS-CoV-1, strain SARS-FRA1), and Severe Acute Respiratory Syndrome Coronavirus 2 (SARS-CoV-2 strain München-1.2/2020/984) were propagated in Vero E6 cells, the Middle East Respiratory Syndrome virus (MERS-CoV strain EMC2012) in HuH-7 cells, and the Sandfly Sicilian virus (SFSV, strain Sabin) in Vero B4 cells. All virus stocks were confirmed to be mycoplasma-free. Infection experiments were done either under conditions of biosafety level 2 (BSL-2; EMCV, LACV, RVFV MP-12, SFSV, VSV) or level 3 (BSL-3; RVFV ZH548, MERS-CoV, SARS-CoV-1, SARS-CoV-2).

Screening of haploid embryonic stem cell library with RVFV MP-12

We used a mouse haploid embryonic stem cell (mESC) barcoded-library (complexity: 9.7×10E6), mutagenized with the genetrap retrovirus JZ-BC frame 0, 1, 2 (5). Thawed cells were grown overnight and seeded into seven 15 cm cell culture dishes at a density of 10×10E6 / dish. Four hours later, cells were washed with PBS and infected with RVFV MP-12 at an MOI of 10. As control, 3.9×10E6 genetrap-library cells and AN3-12 parental wild-type cells were seeded in 10 cm dishes, and infected by RVFV MP-12 at MOI 10, or incubated with the according mock supernatant. After 1 h at 37°C, infection was stopped by adding medium on top of the inoculum, and cells were further incubated at 37°C. Every 24 h during the whole screening process, medium was renewed and cell pictures were taken using bright field microscopy. At day 6 and day 13 post-infection (p.i.), surviving cells were trypsinized, seeded at same density for wild-type and genetrap-library cells, and re-infected 4 h later with RVFV MP-12 at MOI 10. At day 17 after the first infection, surviving cells were trypsinized and analysed for genetrap vector integration sites.

Mapping of genomic genetrap vector integration sites

Experimental details of genomic DNA extraction, restriction digest, ring-ligation and inverse PCR with primers located in the genetrap (see Fig. S3A and B), as well as next generation sequencing of integration sites were described previously (27). In short, the cell clones that were resistant to infection with RVFV MP-12 were trypsinized, washed in PBS and incubated overnight in gDNA Lysis buffer (GDLB: 10mM Tris-HCl pH 8.0, 5mM EDTA, 100mM NaCl, 1% SDS, freshly added 1 mg/mL Proteinase K). After treatment with 10µL RNase A (Qiagen) for 1 h at 37°C, genomic DNA was extracted with phenol/chloroform/isoamylalcohol and precipitated with isopropanol. Pellets were washed in 70% ethanol, dissolved in Tris/EDTA (TE) buffer, and the amount of DNA were measured using QuantiFluor dsDNA dye (Promega). An aliquot of 10 µg DNA was digested overnight at 37°C using *Nla*III and *Mse*I restriction enzymes (NEB), purified using Sera Mag Speedbeads (Thermo Scientific), and resuspended in TE buffer. After DNA ring ligation using T4 ligase (Roche) at 16°C overnight, DNAs were linearized by *Sbf*I (NEB) for 2 h at 37°C and further purified using Sera Mag Speedbeads. The integration site was amplified by inverse PCR (iPCR), using KenTaq polymerase (home-made), the primer DS, and one of the index primers (table S1): 3 min at 95°C, 36 cycles of [13 sec at 95°C, 25 sec at 61°C, 1 min 15 sec at 72°C], 5 min at 72°C, keep at 12°C. The iPCR products were visualised on agarose gel, and samples from the retro-library were purified with a Qiagen gel extraction kit.

Purified iPCR products (genetrap-library digested by either *Mse*I or *Nla*III) were quantified with a Nanodrop, and mixed 1:1 to be combined into one Next Generation Sequencing flowcell. Raw reads were trimmed to 50 nt and processed as in the NCBI Gene Expression Omnibus entry GSM2227065 (28). In short, reads were aligned to the genome (mm10) with bowtie (v1.2.2) (29). Insertions of disruptive and undisruptive regions of each gene are summed up (see Fig. S4). Binomial test of disruptive insertions against undisruptive regions and against disruptive insertions of a retrovirus input (GSM2227065), respectively, was performed for each gene. Genes were ranked by counts of disruptive insertions (DI) and were selected with a LOFscore <= 1e-20 (loss of function score). If the LOFscore equals 0, we remove genes with less than 10 DIs and without insertions in the background.

Growth competition assay

Genetrap-mutagenized clones from the Haplobank collection (www.haplobank.at; (5)) were thawed, grown in 10 cm dishes, and split in 6 wells of a 24-well plate. Three of the wells were infected with a MLP-puro-GFP retrovirus, and 3 were infected with a MLP-mCherry-puro-Cre retrovirus (inducing flipping of the genetrap) (5). At 24 h p.i., 1 µg/mL puromycin (Invitrogen) were added and 5 days later cells were split and aliquots were frozen.

For each gene of interest, cells of one GFP-labelled (original clone) and one mCherry-labelled (flipped sister-clone) version were mixed at a ratio of ~30% knockout cells to ~70% wild-type cells, respectively. At 4 h post-seeding, the mixed cells were washed with DMEM and either mock-infected or infected

with RVFV MP-12 at MOI 5 for 1 h at 37°C. Medium (ESCM) was then added on top, and cells were further incubated at 37°C. Cells were trypsinized at 2 and 5 days pi, and either fixed in 4% PFA for flow cytometry analysis, or further grown after seeding in a new 24-well plate. The initial ratios between GFP and mCherry-labelled cells were confirmed, followed over-time by flow-cytometry (BD FACS LSR Fortessa, with HTS) and analysed with the FlowJo software. Only conditions with more than 1,000 acquired events were taken into account for final analysis.

siRNA knockdown

A549 or Calu-3 cells were seeded in 6-well plates and reverse-transfected with LRP1 siRNAs Hs_LRP1_1 (SI00036190), Hs_LRP1_2 (SI00036197), Hs_LRP1_3 (SI00036204), and Hs_LRP1_5 (SI03109400) (FlexiTube GeneSolution, Qiagen) using Lipofectamine RNAiMAX reagent (Life Technologies), according to the supplier's protocol. A second reverse-transfection was done 2 days later, and the cells seeded in 12-well plates before infection on the following day

Generation of CRISPR-hSpCas9 knockout of HuH-7 cells

HuH-7 cells with a knockout in genes of interest were generated using the CRISPR-hSpCas9 strategy from the Zhang lab (30, 31). For the LRP1 gene, sgRNAs (see table S2) were designed using online tools (https://www.addgene.org/crispr/; http://www.e-crisp.org/E-CRISP/designcrispr.html). After cloning of the required plasmids, the lentiviruses expressing either the specific CRISPR-hSpCas9-sgRNAs or the no template control (NTC) CRISPR-hSpCas9 were generated, and then transduced in triplicates into HuH-7 cells. Clonal cell populations were isolated by limiting dilution, following the Addgene protocol (https://www.addgene.org/protocols/limiting-dilution/). Each single colony was further amplified, and screened by western blot. The control cells HuH-7 NTC (clone E5) and the HuH-7 LRP1 knockout cells (clones C5, C8, E3) were then used in further experiments.

Reverse-transcription and quantitative PCR (RT-qPCR)

Total RNA was extracted from cell lysates using RNeasy (Qiagen) and an aliquot of 100 ng was reverse transcribed with the PrimeScript RT Reagent Kit with gDNA Eraser (Takara) and the included primer mix. An aliquot of 10 ng cDNA was used as template for amplifying sequences of human *GAPDH*, and *LRP1* and VSV with corresponding QuantiTect primers (Qiagen) or specific primers (table S3), respectively, and the SYBR premix Ex Taq (Tli RnaseH Plus) kit (Takara). *RRN18S* was amplified in a similar manner, but with 2 ng cDNA as template. RNA levels of EMCV, LACV MERS-CoV, RVFV, SARS-CoV-1, SARS-CoV-2, and SFSV were detected using specific primers and Taqman probes (table S3), and the Premix Ex Taq (probe qPCR) kit (Takara). All PCRs were performed in a StepOne plus instrument (Applied Biosystems). The values obtained for each gene were normalized against GAPDH mRNA levels (or RRN18S mRNA levels in the case of the VSV RNA) using the threshold cycle ($\Delta\Delta C_T$) method (32).

Immunoblot analysis

Cells were washed with PBS and lysed in Tissue Protein Extraction Reagent (T-PER, Thermo Scientific) containing protease inhibitors (cOmplete tablets EasyPack, Roche), according to the supplier's protocol. Samples for immunodetection of LRP1 were mixed with 4× sample buffer (143 mM Tris-HCl pH 6.8 (Acros), 4.7 % SDS (Roth), 28.6 % glycerol (Roth), 4.3 mM bromophenol blue (Roth)), while samples for detection of RVFV N or SARS-CoV-2 N additionally contained 20% beta-mercaptoethanol, and incubated for 10 min at 105°C.

For detection of LRP1, samples were run through Criterion XT Tris-acetate precast gels (3-8% gradient) (Biorad) in a XT tricine buffer (Biorad), for 1 h 20 min at 150V. Proteins were transferred on an EtOH-activated polyvinylidene fluoride (PVDF) membrane (Millipore) by wet blotting overnight at 40 mA and 4°C, using Tris-glycine transfer buffer (5.8 g/L Tris (Acros), 2 g/L glycine (Roth), 10% absolute EtOH (Roth)). The LRP1 α-chain (515 kDa) and β-chain (85 kDa) were detected using antibodies 8G1 (2µg/mL) (Merck-Millipore) and 5A6 (2µg/mL) (Merck-Millipore) respectively, and a horseradish peroxidase (HRP)-conjugated goat anti-mouse antibody (1:20,000) (Thermo Fisher).

For detection of RVFV N or SARS-CoV-2 N proteins, the samples were run through a home-made 12% SDS-PAGE gel for 1 h at 200V. Proteins were transferred on a MeOH-activated polyvinylidene fluoride (PVDF) membrane (Millipore) by semidry blotting for 1 h at 10V, using semidry blotting buffer (48 mM Tris (Acros), 39 mM glycine (Roth), 1.3 mM SDS (Roth), 20% MeOH (Roth)). The RVFV N was detected by the 10A7 antibody at 1.2ng/µL (kindly provided by A. Brun, INIA, Spain), and a horseradish peroxidase (HRP)-conjugated goat anti-mouse antibody (1:20,000) (Thermo Fisher). The SARS-CoV-2 N was detected by the anti-SARS-CoV nucleocapsid antibody (Biomol, ref 200-401-A50), and a horseradish peroxidase (HRP)-conjugated goat anti-rabbit antibody (1:20,000) (Thermo Fisher). Loading controls were performed by using an anti-tubulin antibody (1:4.000) (abcam, ref ab6046), and a horseradish peroxidase (HRP)-conjugated goat anti-rabbit antibody (1:20,000) (Thermo Fisher). Imunosignals were visualized using the SuperSignal West Femto kit (Pierce), and a ChemiDoc imaging system (Bio-Rad).

Infection time course analysis

Subconfluent cell monolayers were washed once with PBS, incubated 1 h at 4°C with the respective virus or a mock control and again washed 3 times with PBS. Samples for analysis of virus attachment were directly collected by incubating in RLT buffer (Qiagen) for 10 min at room temperature, resuspension, and storage at 4°C until RNA extraction. For analysis of the subsequent replication steps, medium was added and the cells were further incubated at 37°C. For the entry step, cells were washed once in PBS at 2 h p.i., incubated in trypsin-EDTA for 10 min (A549, Calu-3) or 3 min (HuH-7) to remove residual attached viral particles, and then washed 3 times in PBS with centrifugations (5 min at 10,000 g). Cell pellets were resuspended in RLT buffer and stored at 4°C. At 5 h and 24 h p.i., cells

were washed once with PBS, incubated with RLT buffer for 10 min at room temperature, resuspended, and stored at 4°C.

Virus titration

Supernatants of infected cells were collected and cleared by centrifugation at 400 g for 5 min. Serial dilutions were made to infect subconfluent Vero E6 monolayers, and infected cells were then incubated in medium containing 1.5 % Avicel for 3 days. Cells were washed twice in PBS and stained for 10 min with a cristal violet solution (0.75% crystal violet, 3.75% folmaldehyde, 20% ethanol, 1% methanol). Cells were then washed, and plaques were counted. Titers were determined as Plaque Forming Units (PFU) per ml.

Statistical analysis

Statistical analyses performed are described in the figure legends.

Acknowledgements

We are indebted to Christian Drosten and Marcel Müller for kindly providing the SARS-CoV-2 virus and Calu-3 cells, respectively, and to Andreas Leibbrandt, Ellen Wetzel, Manuela Kinzer and Nicole Schuller for helpful discussions and technical support. Work in the authors' laboratories was funded by the Bundesministerium für Bildung und Forschung (Infect-ERA, grant "ESCential") (FW, AM, JP), the Swedish Research Council (VR; no. 2018-05766) (FW, AM, JP), the European Union's Horizon 2020 research and innovation program under grant agreement no. 101005026 (MAD-CoV-2) (FW, AM, JP), and the Pandemie Netzwerk Land Hessen (FW).

Author contributions

Conceptualization: SD, AM, UE, JMP, FW
Methodology: SD, AM, UE, JMP, FW
Investigation: SD, TWS, TB, PS
Visualization: SD, TWS, AM, UE, JMP, FW
Funding acquisition: AM, JMP, FW
Project administration: AH, JMP, FW
Supervision: UE, JMP, FW
Writing – original draft: FW
Writing – review & editing: SD, TB, AH, AM, UE, JMP, FW

Conflicts of interest

The authors declare that there are no conflicts of interest.

Data and materials availability

All data are available in the main text or the supplementary materials.

References

1. S. D. Judson *et al.*, Translating Predictions of Zoonotic Viruses for Policymakers. *Ecohealth* **15**, 52-62 (2018).
2. WHO (2021) Prioritizing diseases for research and development in emergency contexts.
3. F. Zhang *et al.*, Global discovery of human-infective RNA viruses: A modelling analysis. *PLoS Pathog* **16**, e1009079 (2020).
4. D. Wright, J. Kortekaas, T. A. Bowden, G. M. Warimwe, Rift Valley fever: biology and epidemiology. *J Gen Virol* **100**, 1187-1199 (2019).
5. U. Elling *et al.*, A reversible haploid mouse embryonic stem cell biobank resource for functional genomics. *Nature* **550**, 114-118 (2017).
6. V. Actis Dato, G. A. Chiabrando, The Role of Low-Density Lipoprotein Receptor-Related Protein 1 in Lipid Metabolism, Glucose Homeostasis and Inflammation. *Int J Mol Sci* **19** (2018).
7. M. Franchini, M. Montagnana, Low-density lipoprotein receptor-related protein 1: new functions for an old molecule. *Clin Chem Lab Med* **49**, 967-970 (2011).
8. S. L. Gonias, W. M. Campana, LDL receptor-related protein-1: a regulator of inflammation in atherosclerosis, cancer, and injury to the nervous system. *Am J Pathol* **184**, 18-27 (2014).
9. B. van de Sluis, M. Wijers, J. Herz, News on the molecular regulation and function of hepatic low-density lipoprotein receptor and LDLR-related protein 1. *Curr Opin Lipidol* **28**, 241-247 (2017).
10. L. Wujak, P. Markart, M. Wygrecka, The low density lipoprotein receptor-related protein (LRP) 1 and its function in lung diseases. *Histol Histopathol* **31**, 733-745 (2016).
11. A. M. Riblett *et al.*, A Haploid Genetic Screen Identifies Heparan Sulfate Proteoglycans Supporting Rift Valley Fever Virus Infection. *J Virol* **90**, 1414-1423 (2016).
12. M. Kainulainen, S. Lau, C. E. Samuel, V. Hornung, F. Weber, NSs Virulence Factor of Rift Valley Fever Virus Engages the F-Box Proteins FBXW11 and beta-TRCP1 To Degrade the Antiviral Protein Kinase PKR. *J Virol* **90**, 6140-6147 (2016).
13. R. Mudhasani *et al.*, Protein Kinase R Degradation Is Essential for Rift Valley Fever Virus Infection and Is Regulated by SKP1-CUL1-F-box (SCF)FBXW11-NSs E3 Ligase. *PLoS Pathog* **12**, e1005437 (2016).
14. Z. He, G. Wang, J. Wu, Z. Tang, M. Luo, The molecular mechanism of LRP1 in physiological vascular homeostasis and signal transduction pathways. *Biomed Pharmacother* **139**, 111667 (2021).
15. S. S. Ganaie *et al.*, Lrp1 is a host entry factor for Rift Valley fever virus. *Cell* **184**, 5163-5178 e5124 (2021).
16. S. Miller, J. Krijnse-Locker, Modification of intracellular membrane structures for virus replication. *Nat Rev Microbiol* **6**, 363-374 (2008).
17. G. Wolff, C. E. Melia, E. J. Snijder, M. Barcena, Double-Membrane Vesicles as Platforms for Viral Replication. *Trends Microbiol* **28**, 1022-1033 (2020).
18. G. Wolff *et al.*, A molecular pore spans the double membrane of the coronavirus replication organelle. *Science* **369**, 1395-1398 (2020).
19. V. Coronaviridae Study Group of the International Committee on Taxonomy of, The species Severe acute respiratory syndrome-related coronavirus: classifying 2019-nCoV and naming it SARS-CoV-2. *Nat Microbiol* **5**, 536-544 (2020).
20. R. F. Clayton *et al.*, Liver cell lines for the study of hepatocyte functions and immunological response. *Liver Int* **25**, 389-402 (2005).

21. T. Marjot *et al.*, COVID-19 and liver disease: mechanistic and clinical perspectives. *Nat Rev Gastroenterol Hepatol* **18**, 348-364 (2021).
22. A. Saviano, F. Wrensch, M. G. Ghany, T. F. Baumert, Liver Disease and Coronavirus Disease 2019: From Pathogenesis to Clinical Care. *Hepatology* **74**, 1088-1100 (2021).
23. Y. Wang *et al.*, SARS-CoV-2 infection of the liver directly contributes to hepatic impairment in patients with COVID-19. *J Hepatol* **73**, 807-816 (2020).
24. M. Uhlen *et al.*, Proteomics. Tissue-based map of the human proteome. *Science* **347**, 1260419 (2015).
25. M. Karlsson *et al.*, A single-cell type transcriptomics map of human tissues. *Sci Adv* **7** (2021).
26. U. Elling *et al.*, Forward and Reverse Genetics through Derivation of Haploid Mouse Embryonic Stem Cells. *Cell Stem Cell* **9**, 563-574 (2011).
27. U. Elling *et al.*, Derivation and maintenance of mouse haploid embryonic stem cells. *Nat Protoc* **14**, 1991-2014 (2019).
28. T. Burkard (2017) Retrovirus-EGT. (NCBI, Gene Expression Omnibus).
29. B. Langmead, C. Trapnell, M. Pop, S. L. Salzberg, Ultrafast and memory-efficient alignment of short DNA sequences to the human genome. *Genome Biol* **10**, R25 (2009).
30. N. E. Sanjana, O. Shalem, F. Zhang, Improved vectors and genome-wide libraries for CRISPR screening. *Nat Methods* **11**, 783-784 (2014).
31. O. Shalem *et al.*, Genome-scale CRISPR-Cas9 knockout screening in human cells. *Science* **343**, 84-87 (2014).
32. K. J. Livak, T. D. Schmittgen, Analysis of relative gene expression data using real-time quantitative PCR and the 2(T)(-Delta Delta C) method. *Methods* **25**, 402-408 (2001).

Figures

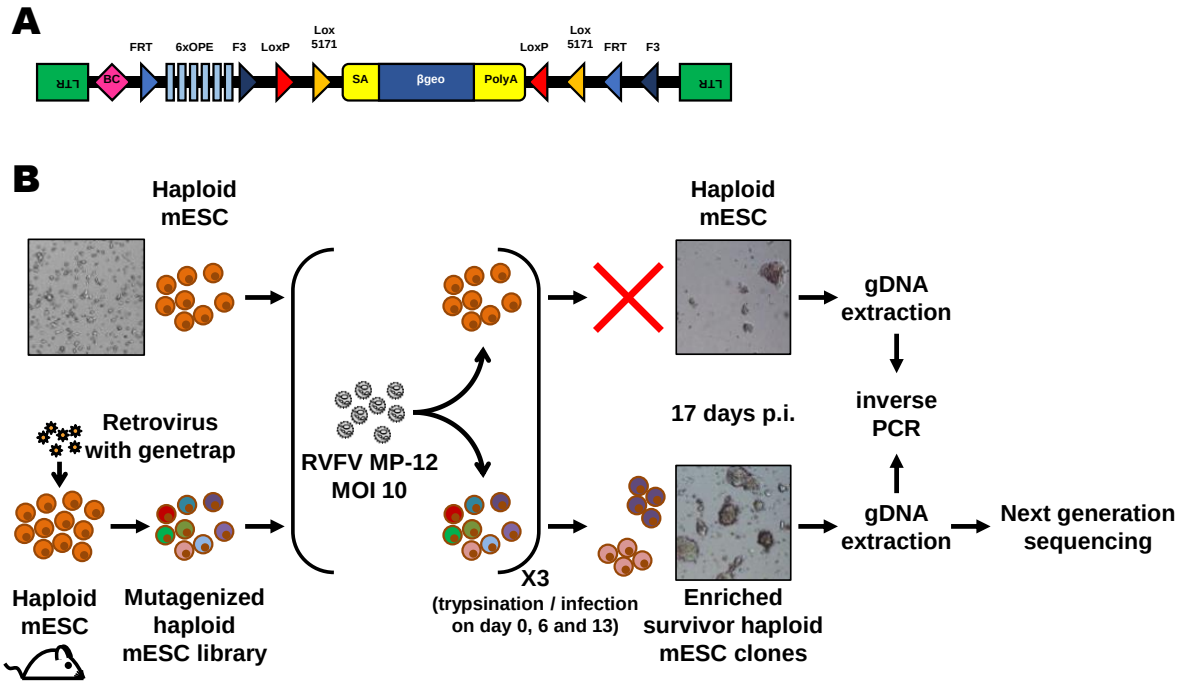

Figure 1. Forward genetics screen of the haploid mouse embryonic stem cell library for resistance to RVFV MP-12. (A) Schematic representation of the retroviral revertible genetrap used for mutagenesis. BC, barcode; OPE, Oct4 binding sites; SA, splicing acceptor site. (B) Experimental workflow for the RVFV MP-12 resistance screen using insertional mutagenesis. Bright-field microscopy images of the cells before infection and at the end of the screening process are shown as examples. mESC, mouse embryonic stem cells; p.i, post-infection; RVFV, Rift Valley fever virus.

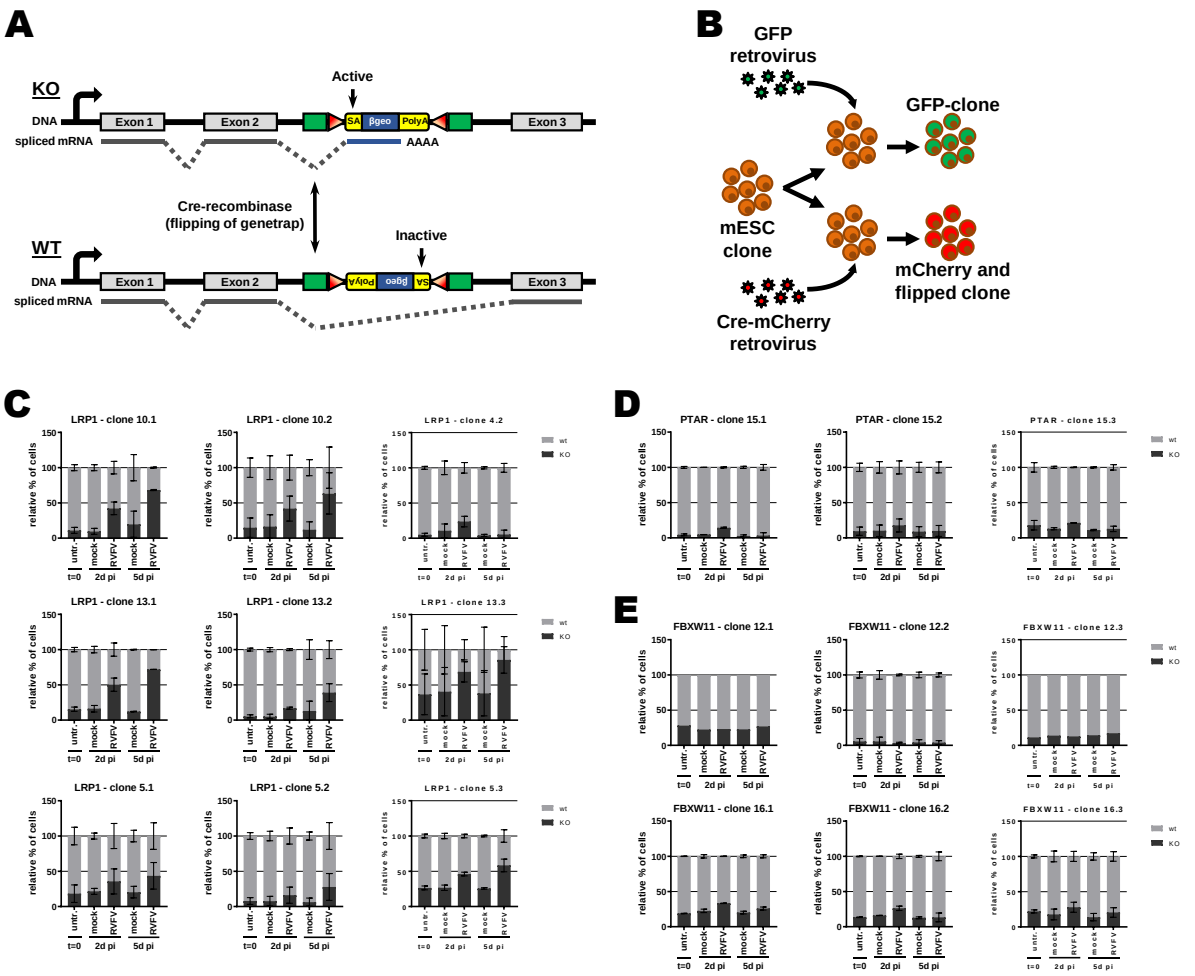

Figure 2. Growth competition assay in mouse embryonic stem cells. (A) Schematic representation of the genetrap system when inserted into an intron. When in sense orientation, the genetrap exposes a splicing acceptor site and will be inserted into the mature mRNA, leading to a knockout of the gene of interest. When in antisense orientation, the splicing acceptor site is inactive and the genetrap will be spliced out, leading to a wild-type expression of the gene of interest. Flipping of the genetrap orientation is possible by expressing the Cre-recombinase. (B) Schematic representation of the assay. Cell clones with a genetrap present in an intron of the gene of interest were selected from the Haplobank. One sub-population was transduced with a GFP retrovirus, preserving the genetrap in its original orientation, and one sub-population was transduced with a Cre recombinase mCherry retrovirus, which flips the genetrap orientation. The GFP clone and the Cre-mCherry clone are sister clones. Each transduction (GFP / Cre-mCherry) was done in triplicates. (C, D, E) Growth competiton assay between sister clones bearing a genetrap into the gene of interest (C: LRP1, D: PTAR, E: FBXW11). Sister clones with wild-type phenotype are in grey and sister clones with knockout phenotype are in black, independently of the GFP/Cre-mCherry transduction (see table 1). Approximatively 30% of knockout cells were mixed with 70% of their wild-type sister clone, and infected with RVFV MP-12 at MOI 5. Ratio between both sister clones was followed by flow cytometry. n=2, except if event count was below 1,000, in which case the whole data set was removed (n=1)

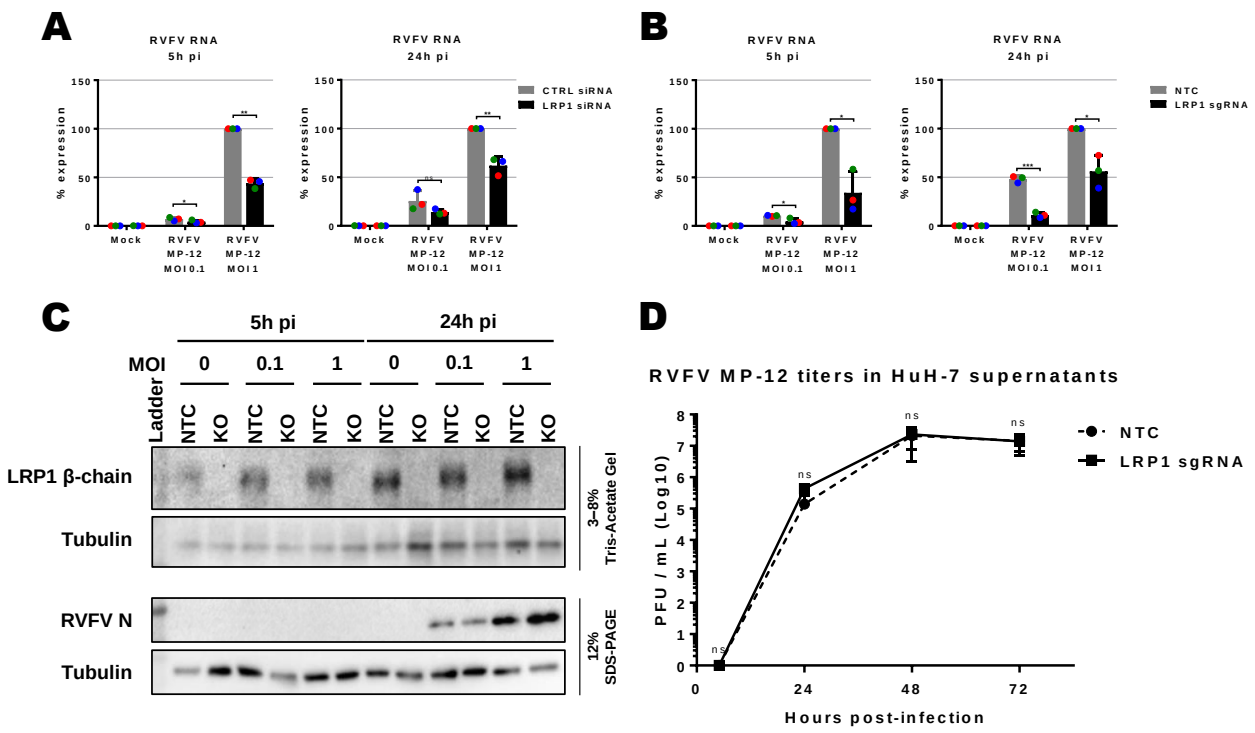

Figure 3. Influence of LRP1 downmodulation on RVFV MP-12. Virus RNA levels were measured in A549 knockdown for LRP1 (A) and HuH-7 knockout for LRP1 (B). Cells were infected in a synchronized manner with RVFV MP-12 at MOI 0.1 or MOI 1 as indicated, and RNA was extracted at 5 h and 24 h post-infection (p.i.). Two-step RT-qPCR was done to detect RVFV MP-12 RNA (L-segment) and the GAPDH reference gene. The RNA levels of RVFV L-segment in the control (CTRL) siRNA or no template control (NTC) CRISPR/Cas9 cells infected at MOI 1 were set to 100%. (C) LRP1 knockout HuH-7 cells were infected with RVFV MP-12 at MOI 0.1 or MOI 1, lysed at 5 h and 24 h p.i., and subjected to immunoblotting as indicated. A representative blot is shown. (D) HuH-7 CRISPR/Cas9 cells (NTC or LRP1 knockout) were infected with RVFV MP-12 at MOI 0.01, supernatants harvested at the indicated time points, and infectious virus measured by plaque assay. Statistics were done on 3 independent experiments, using a paired and 1-tail Student t-test on log-transformed data: *, $p<0.05$; **, $p<0.01$; ***, $p<0.001$; n.s., non-significant.

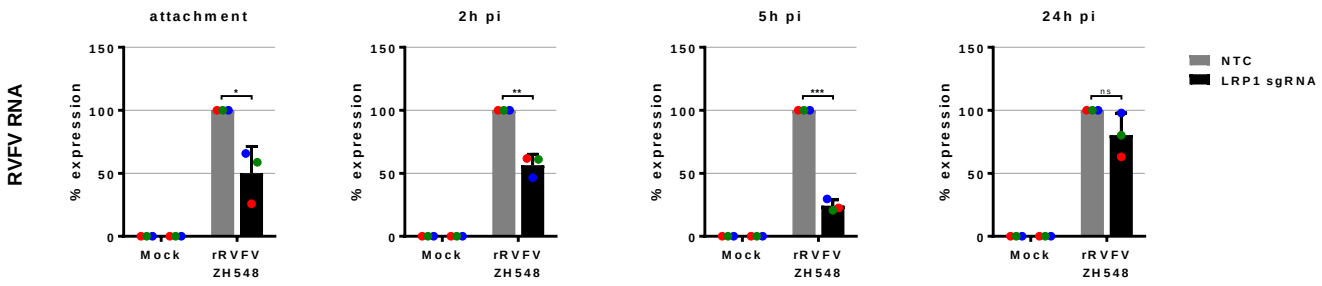

Figure 4. Virus RNA levels in LRP1 knockout cells over the course of infection with RVFV strain ZH548. HuH-7 LRP1 knockout cells and HuH-7 NTC (no template control) cells were infected in a synchronized manner at MOI 1, washed 3 times, and further incubated in medium. Samples were collected after the 3 washes post-infection (attachment step), or at 2 h, 5 h or 24 h post-infection. Two-step RT-qPCR was done to detect viral RNA, as well as the GAPDH reference gene. The RNA levels in the infected NTC cells was set to 100%. Statistics were done on 3 independent experiments, using a paired and 1-tail Student t-test: *, $p<0.05$; **, $p<0.01$; ***, $p<0.001$; n.s., non-significant.

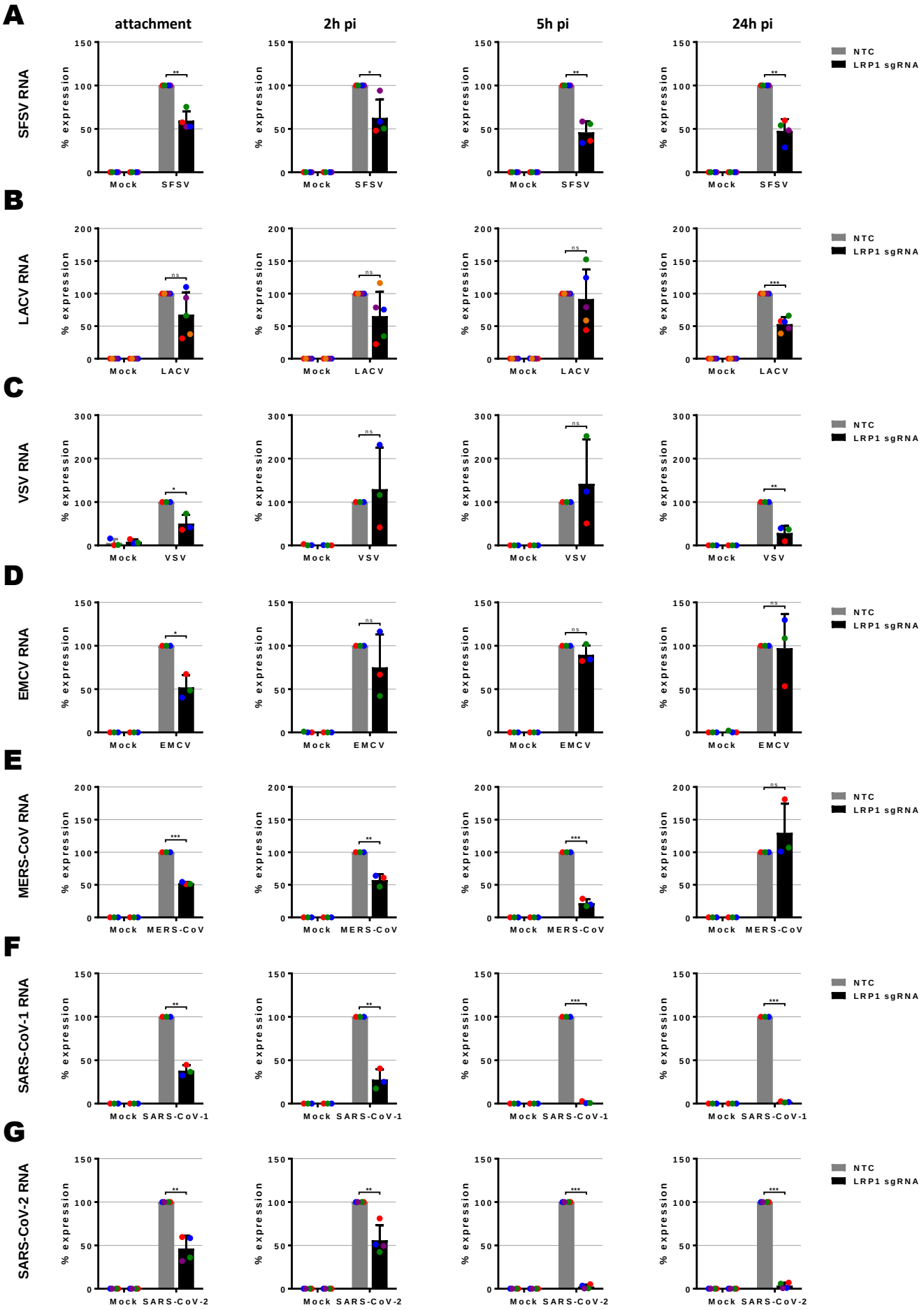
A
B
C
D
E
F
G
attachment
2h pi
5h pi
24h pi
SFSV RNA
LACV RNA
VSV RNA
EMCV RNA
MERS-CoV RNA
SARS-CoV-1 RNA
SARS-CoV-2 RNA
% expression
Mock
SFSV
LACV
VSV
EMCV
MERS-CoV
SARS-CoV-1
SARS-CoV-2
NTC
LRP1 sgRNA

Figure 5. Virus RNA levels in LRP1 knockout cells over the course of infection. (A) Sandfly Sicilian virus (SFSV), (B) LaCrosse virus (LACV), (C) Vesicular stomatitis virus (VSV), (D) encephalomyocarditis virus (EMCV), (E) Middle east respiratory syndrome virus (MERS-CoV), (F) Severe Acute Respiratory Syndrome coronavirus 1 (SARS-CoV-1), (G) Severe Acute Respiratory Syndrome coronavirus 2 (SARS-CoV-2). HuH-7 LRP1 knockout cells and HuH-7 NTC (no template control) cells were infected with the various viruses at MOI 1, except for VSV that was used at MOI 0.1, washed 3 times and further incubated in medium. Samples were collected after the 3 washes post-infection (attachment step), or at 2 h, 5 h or 24 h post-infection. Two-step RT-qPCR was done to detect viral RNA, as well as the GAPDH and 18S rRNA reference genes. The RNA levels in the infected NTC cells was set-up to 100%. Statistics were done on 3, 4, or 5 independent experiments, using a paired and 1-tail Student t-test: *, $p<0.05$; **, $p<0.01$; ***, $p<0.001$; n.s., non-significant.

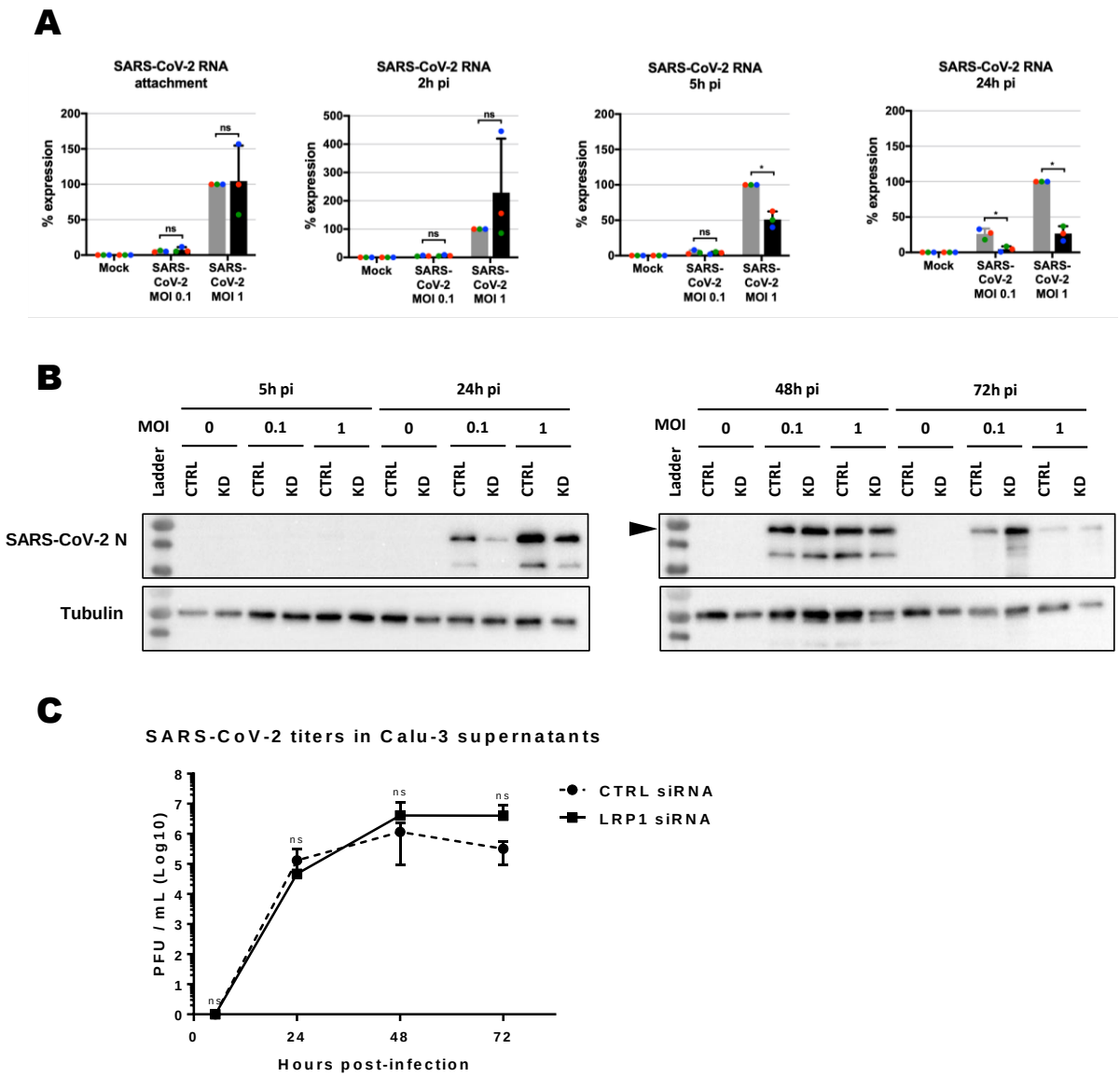

Figure 6. Effect of LRP1 knockdown on SARS-CoV-2 multiplication in Calu-3 lung cells. siRNA-transfected cells were infected at the two indicated MOIs, samples for viral RNA analysis (A), immunoblotting (B) and virus yields (MOI 0.01) (C) were taken at the different time points, and analyzed as described for figures 3 to 5. A representative blot is shown in (B). Statistics were done on 3 independent experiments, using a paired and 1-tail Student t-test on log-transformed data: *, $p<0.05$; **, $p<0.01$; ***, $p<0.001$; n.s., non-significant.

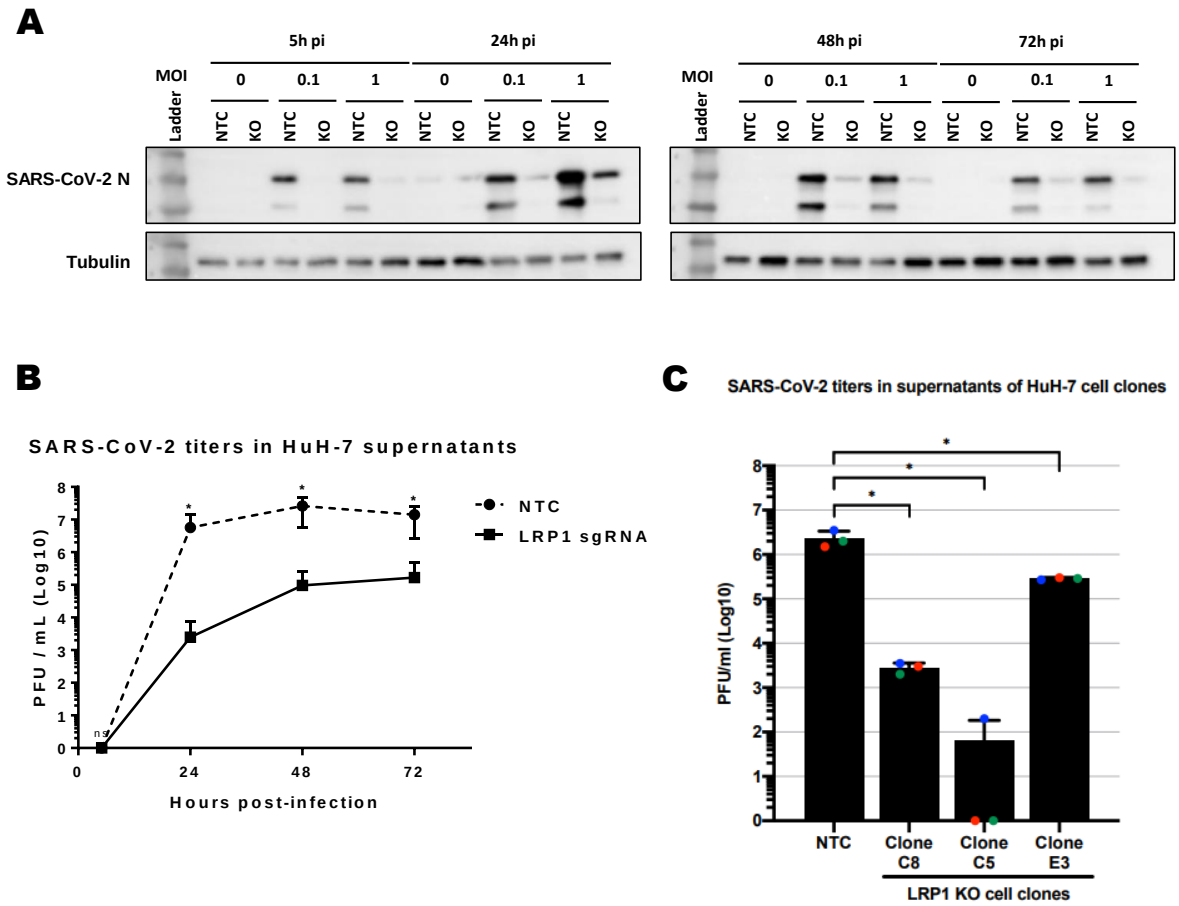

Figure 7. Effect of LRP1 knockout on SARS-CoV-2 multiplication in HuH-7 hepatocytes. Cells were infected at the two indicated MOIs, and samples for immunoblotting (A) and virus yields (MOI 0.01) (B) were taken at the different time points, and analyzed as described for figures 3 C and D. (C) Comparison of different HuH7 cell clones with CRISPR/Cas9 knockout of LRP1. Cells had been infected at an MOI of 0.01 and virus yields measured 24 h later. C8 is the LRP1 knockout cell clone used in all other experiments with HuH-7 cells. Representative blots are shown in (A). Statistics were done on 4 (B) or 3 (C) independent experiments, using a paired 1-tailed Student's t-test (B) or one-way ANOVA with Dunnett correction for multiple comparisons (C) on log-transformed data: *, $p<0.05$; **, $p<0.01$; ***, $p<0.001$; n.s., non-significant.

Gene	Clone #	Ref. Haplobank	Mutagen	Genetrap orientation	GFP	Cre-mCherry
Lrp1	4	00800IE06	retroviral	antisense	wt	KO
	5	01128IH08	transposon	sense	KO	wt
	10	00354IA04	lentiviral	sense	KO	wt
	13	00561IB08	retroviral	sense	KO	wt
Ptar	15	01224IG10	transposon	antisense	wt	KO
Fbxw11	12	00371IH05	lentiviral	sense	KO	wt
	16	01258IE05	transposon	antisense	wt	KO

Table 1. List of clones from the Haplobank collection (mouse haploid embryonic stem cells, AN3-12)